Digital light processing-3D printing of thermoset materials with high biodegradability from amino acid-derived acrylamide monomers

Isaac Isarn[a], Ľudmila Hodásová[b,c,d], Maria M. Pérez-Madrigal[b,d], Francesc Estrany[b,d] Elaine Armelin[b,d,*], Fernando Bravo[a,*]

[a)] ICIQ-CERCA – Institute of Chemical Research of Catalonia, The Barcelona Institute of Science and Technology, Avinguda dels Països Catalans 16, 43007, Tarragona, Spain.

[b)] IMEM-BRT Group, Departament d'Enginyeria Química, EEBE, Universitat Politècnica de Catalunya, C/ Eduard Maristany, 10-14, Ed. I, 2nd floor, 08019, Barcelona, Spain.

[c)] CIEFMA Group, Departament de Ciència i Enginyeria de Materials, , EEBE, Universitat Politècnica de Catalunya, C/ Eduard Maristany, 10-14, Building I, 1st floor, 08019, Barcelona, Spain.

[d)] BRCMSE - Barcelona Research Center in Multiscale Science and Engineering, Universitat Politècnica de Catalunya, C/ Eduard Maristany, 10-14, basement S-1, 08019, Barcelona, Spain.

[*]Corresponding authors: fbravo@iciq.cat and elaine.armelin@upc.edu

Abstract

Six acrylamide resins, derived from L-phenylalanine and L-leucine, have been designed for application in DLP printers to obtain biodegradable thermoset polymers. The acrylamide copolymers were prepared under light irradiation at 405 nm and thermal post-curing processes. Low molecular weight poly(ethylene glycol)diacrylate (PEGDA) and *N*,*N*-dimethylacrylamide (DMAM), both liquid resins, were used as co-monomers and diluents for the amino acid-derived acrylamide solubilization. The presence of two phenylalanine units and two ester groups in the acrylamide monomer accused a fast degradation rate in hydrolytic medium in 90 days. The residual products leached in the aqueous media proved to be non-cytotoxic, when 3D-printed samples were cultured with osteoblast cells (MG63), which represents an advantage for the safe disposal of printer waste materials. The scaled-up pieces derived from L-phenylalanine and diethyleneglycol, as amino acid-derived acrylamide (named compound **C**), PEGDA and DMAM, presented high dimensional stability after DLP printing of complex structures used as testing samples. Layers of 50 μm of thickness were well cohesive having isotropic behaviour, as demonstrated with tensile-strain measurements performed in X-Y-Z (plane) directions. The compound **C**, which contains phenylalanine amino acid, revealed a promising potential to replace non-biodegradable acrylate polymers used in prototyping systems.

Keywords: acrylamide resins, poly(ethylene glycol)diacrylate, digital light processing, biodegradability, cytotoxicity.

1. Introduction

The search for new functional materials is a topic of continuous research. In particular, the global goals for sustainable development are leading the scientific community to promote the use of bio-sustainable resins and easy-to-biodegrade plastics to reduce the impact of waste generation,[1] thus, closing the life-cycle assessment of such plastic transformation processes, which has derived in the concept of circular economy in additive manufacturing.[2–4]

Despite natural amino acids have traditionally been considered as prominent members of the chiral pool for the enantioselective synthesis of small molecules, the use of amino acids as biosourced materials is relatively scarce, though it may be expected that they will come into force towards the preparation of novel materials in the next years.[5] Recently, a new unsaturated polyesteramide (UPEA), derived from L-phenylalanine, has been synthesized as a promising raw material for 3D-printing technology thanks to its ease of degradation in an enzymatic medium.[6–9] The acrylamide bonds in this polymer were cross-linked with poly(ethyleneglycol) diacrylate (PEGDA) by the light-promoted formation of radicals, to provide a cured material that, besides the presence of biosourced phenylalanine, had good biodegradable properties due to the ester and amide moieties in the polymer chain. Such groups are usually the target of lipases' attack. However, the synthetic route to obtain UPEA is too long and unfeasible for scale-up.[6,9] From an industrial point of view, the components of the photo-curable resin should be easily available at a sufficient scale.

Recently, Voet and co-workers[10] have compiled the ultimate development of sustainable photocurable liquid resins, for stereolithography (SLA) and digital light processing (DLP) technologies, to reduce the environmental footprint of additive manufacturing. Among the promising possibilities of resins for SLA uses, such as that derived from lignin, vegetable oils and ethers; PEG is described to be one powerful candidate. It has been demonstrated to have good biodegradability and bioresorbable properties. The polymer actuates as an initiator, accelerating the radical polymerization, and as a reactive diluent, when combined with other comonomers.[11–13] Furthermore, PEGDA has proved biocompatibility and non-cytotoxic responses in 3D-printing manufacturing, if properly UV absorbers are employed, as recently reported by Warr *et al*.[14] This polyether-acrylate has been also mixed with acrylamide (AAm) monomers, in

DLP-based multimaterial 3D printing apparatus, to prepare stretchable hydrogels by using high efficiency photoiniators.[15,16] In this way, Ge *et al*.[16] described a printed shape-memory polymer hydrogel stent, composed by AAm, PEGDA, and 2,4,6-trimethylbenzoyl diphenylphosphine oxide (TPO) photoinitiator, charged with red dye as "drug"; being able to control the drug delivery by following the expansion of the stent.

The previously reported materials are examples of a photo-cured compound *via* free radical polymerization. In the last decade, there was an explosion of novel materials and applications of SLA and DLP printed objects,[17,18] because the complexity and resolution of the printed pieces with these techniques are among the best compared to other 3D printing techniques.[19] Unfortunately, the biodegradability of polyether polymers are not so high as in the case of polyesters (such as PLA, PLGA or PCL polymers).[20][21] Becker and co-workers, for example, recently described the 3D printing of fully bioresorbable implants made of poly(propylene fumarate) tri-block copolymer composites.[22] The hydrolytic degradation was activated by the presence of labile thiol crosslinker molecules. Therefore, it opens new possibilities for fast prototyping of bioresorbable implants. However, it is important to design monomers with functionalities that have high affinity to either water or enzymes, to favour the biodegradability of the 3D printed pieces.

The present work reports the synthesis of novel acrylamide resins, with amino acid groups, in order to provide a suitable liquid and homogeneous solution for DLP printing of biodegradable materials. It was considered necessary to reduce the molecular size of the components of the UPEA polymer to its basic constituents, thus designing a difunctional monomer, which can be further cross-linked, and that keeps all the bond type features of UPEA.[9] Furthermore, due to their much smaller molecular weight, it is prone to be more easily solubilized in other liquid monomer resins, employed as diluents (such as PEGDA), which is usually one of the most important monomer (or co-monomer) used in acrylate systems.[23]

In summary, the objective was to develop a new formulation with different acrylamide monomers that could provide photo-cured materials with good reaction kinetics and biodegradability properties. The acrylamide/ester-PEGDA monomer mixtures should cure in DLP printers with reasonable printing times and with good level of resolution. With this purpose in mind, the goal is to be able to print thin layers of 50 μm of polymer

with a high-quality resolution by using a DLP printer and evaluate the final piece properties, such as mechanical resistance, enzymatic degradation and biocompatibility.

2. Experimental procedure

2.1. Materials

Boc-L-phenylalanine was purchased from Bachem. L-*tert*-leucine and 1-Ethyl-3-(3′-dimethylaminopropyl)carbodiimide·HCl (EDC·HCl) were supplied by Fluorochem. Trifluoroacetic acid and *trans*-2-Butene-1,4-diol were provided by ABCR GmbH. 4-(Dimethylamino) pyridine and hydrogen chloride, 5-6N solution in 2-propanol, were supplied by Acros Organics. Ethylene glycol, diethylene glycol, poly(ethylene glycol) diacrylate (average Mn 250), and triethylamine were purchased from Sigma Aldrich. Acryloyl chloride was endowed by Alfa Aesar. *N*,*N*-Dimethylacrylamide, phenylbis(2,4,6-trimethylbenzoyl)phosphine oxide (BAPO) and 2,5-bis(5-*tert*-butyl-2-benzoxazolyl)thiophene (UV absorber) were purchased from TCI chemicals. Ethyl acetate, dichloromethane and all the solvents used in the synthesis were provided by Panreac (ITW Reagents). Materials used for photopolymerization tests are described in the supporting file (SI).

2.2. Synthetic route for the preparation of acrylamide resins containing amino acids

The different diacrylamide monomers derived from amino acids were synthesized in a three-step sequence: (1) the reaction between the BOC protected amino acid [L-phenylalanine (**1**) or L-leucine (**2**)] with the diol linker (*E*)-but-2-ene-1,4-diol (**3**), ethylene glycol (**4**) or diethylene glycol (**5**); (2) the deprotection of the amine groups; and (3) the reaction of both terminal free amines with acryloyl chloride to obtain the desired acrylamide monomers coded as numbers **18-23**. A general description of the reaction is depicted in Scheme 1. All products were purified before polymerization (see Supporting Information for synthetic details and route optimization). To the best of authors' knowledge, none of these six monomers represented in Scheme 1 were reported before in the literature.

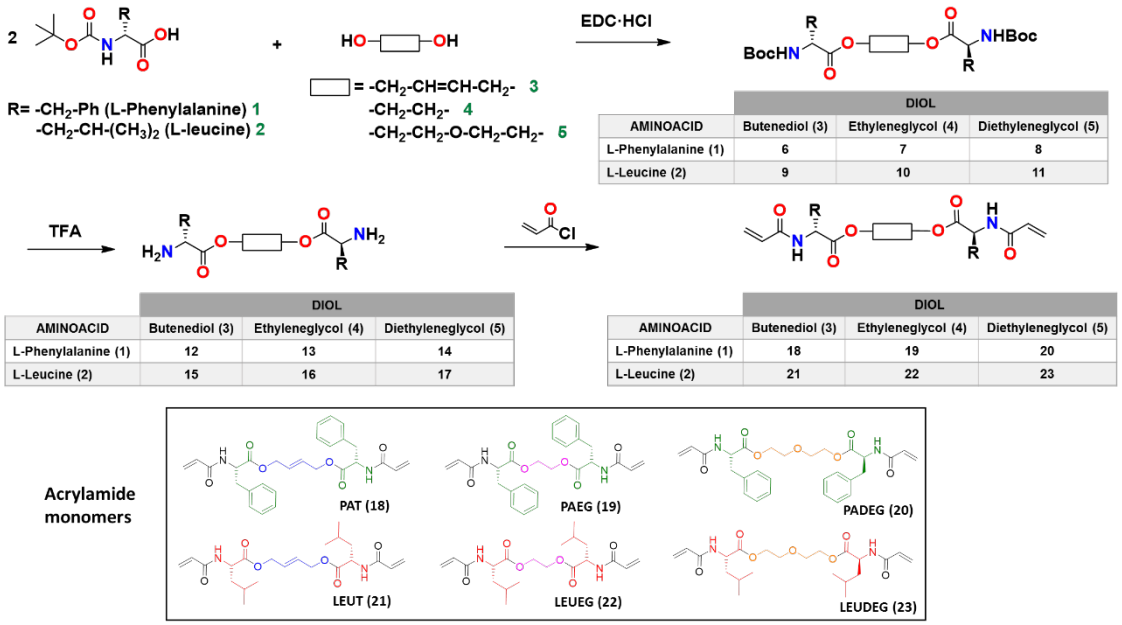

Scheme 1. General scheme of the synthesis of the six acrylamide monomers **18-23**, developed in the present work, by using different side chain groups (R) and diol spacers/linkers.

2.3. Thermoset preparation

Photopolymerization of each of the six synthesized monomers (**18-23**) was conducted separately, in order to obtain crosslinked homopolymers and to check their reactivity. The three phenylalanine derivatives **18**, **19** and **20**, which were obtained as solids at room temperature, were dissolved in the minimum amount of dichloromethane (DCM) and mixed with 0.5 wt. % of BAPO (phenylbis(2,4,6-trimethyl-benzoyl)phosphine oxide) as a photoinitiator for visible- or UV-triggered photopolymerization. In contrast, monomers **21**, **22** and **23** are waxy materials or viscous syrups and lower amount of DCM was needed for their solubilization. Some drops of these solutions were placed on a glass slide and irradiated with a 405 nm LED situated at a distance of about 3 cm at the maximum intensity of 100 mW/cm^2 (measured using a calibrated photodiode). Solid samples were obtained after 1h of UV irradiation.

However, due to the solid or highly viscous nature of the acrylamide monomers **18-23**, not suitable for 3D printer fabrication, the incorporation of liquid co-monomers such as polyethylene glycol diacrylate ($PEGDA_{250}$) and dimethyl acrylamide (DMAM), which act as reactive solvents, was necessary to prepare new thermoset materials with biodegradability and biocompatibility properties.[24–28] In order to obtain full solubility,

the ratio of acrylamide monomer:PEGDA:DMAM was established as 1:2:2.5. To these mixtures, 0.5 wt. % of BAPO was added as the photoinitiator, which is a typical concentration for photocuring, and 0.4 wt. % of 2,5-bis(5-tert-butyl-benzoxazol-2-yl)thiophene was added as a UV photo-absorber. Thus, such mixtures can be expressed by composition in percentages by weight as: 18.02 wt. % of each acrylamide monomer, 36.04 wt. % of PEGDA, 45.04 wt. % of DMAM, 0.5 wt. % of BAPO and 0.4 wt. % of UV absorber. These compounds were mixed under magnetic stirring and the samples were heated at 60 °C to increase the solubilization kinetics. Solubility was accelerated with the aid of a sonication bath, which also served for degassing purposes. The pale-yellow homogeneous solutions were stable upon cooling to room temperature and standing for prolonged time (> 1 month).

Prior to the manufacturing of acrylate prototypes with the 3D DLP printer, the samples were cured in Teflon moulds or between glass slides in order to check the polymerization conversion by FTIR. The curing protocol followed was: (1) a first irradiation (3h) from a 405 nm LED source, which is visible light at the limit with near UV, situated at 3 cm distance (100 mW/cm^2 in power intensity); (2) post-curing (3h) under irradiation at 460 nm (at this wavelength, which has an increased penetration depth, the photo-absorber is not active) at 3 cm distance (500 mW/cm^2 of power intensity); (3) washing the samples with isopropanol in a sonication bath for 30 min, in order to eliminate any unreacted monomers from the polymerized piece; and (4) thermal post-curing at 170 °C for 12h in a vacuum oven. This protocol was used to ensure the maximum achievable degree of conversion and prevent any further polymerization from occurring during the heating cycle required for the dynamic mechanical testing (dynamic mechanical thermal analysis, DMA). Finally, the cured samples were further characterized by spectroscopy and thermal techniques (FTIR, RAMAN, DSC, TGA).

In this work, to facilitate reading, the liquid formulations will be denoted by low case letters from **a** to **f**, and the cured materials will be denoted by capital letters from **A** to **F** (see Table S1, supporting information file**)**.

2.4. 3D printing

The aim of this work was to obtain a novel photocurable resin to be used in a Digital Light Processing (DLP) printer. A commercially available printer (Photon S 3D printer from Anycubic) was used. It is composed of a resin vat (with an FEP-Fluorinated

Ethylene Propylene film) at the bottom and a metallic platform at the upper part where samples are printed on. The resin in the bath receives a 405 nm light irradiation from the bottom of the bath, with a fixed intensity of 0.5 mW/cm^2, measured at the surface of the vat. The photo-polymerization occurs between the resin and the metallic platform, where the samples are printed, avoiding in this way oxygen inhibition, and which allows precise control of the layer thickness. In this step, the curing protocol was the same as that reported for the small samples (section 2.3).

For this step, optimization of the synthesis (Scheme S1) and scale-up production of the raw material were necessary, according to the detailed description reported in supporting file (Annex 1). The composition of acrylamide monomers (amino acid derived and DMAM) and PEGDA, with photoinitiator and UV absorber (in weight percentages), was the same as that mentioned in section 2.3, as well as the post-curing process. With the DLP printer, dumbbell tensile test specimens of dimensions L_0=63.5±X mm, W=3.18±0.5 mm, T=3.2±0.4 mm (Figure S3) were prepared following ASTM D638 type V specimens, as well as the manufacturing of more complex models to evaluate the spatial resolution of the printed pieces with the most prominent acrylamide monomer (**20**).

2.5. Material characterization

2.5.1. Characterization of acrylamide monomers and follow up of crosslinking conversion

The new acrylamide monomers were fully characterized by HPLC, HR-MS, FTIR-ATR and NMR techniques (see section 2.2 in the SI). The liquid mixtures, consisting of acrylamide compounds, PEGDA and DMAM, were evaluated by FTIR-ATR to follow up on the curing process. In FTIR-ATR analysis, the degree of polymerization conversion was followed by using the two absorption bands observed at 826-780 cm^{-1}, which correspond to the out-of-plane vibrations of the =C-H of the acrylate group, and which is almost absent after the polymerization. For phenylalanine monomers (compounds **18**-**20**) a peak at about 695 cm^{-1} (likely the out-of-plane C-H vibration of the aromatic ring), which is present before and after polymerization, was used as a correction factor to determine the conversion by peak areas, as exemplified in Equation 1:

$$[Conversion] = \left[\left(1 - \frac{A_{826-780,C}/A_{695,C}}{A_{826-780,R}/A_{695,R}}\right)\right] \times 100 \qquad \text{(Eq. 1)}$$

being $A_{x,C}$ and $A_{x,R}$ the peak area of the cured materials **A-C** and the liquid resin **a-c**, respectively. For monomers compositions, please, refer to Table S1 (SI file).

Solid samples prepared with 405 nm-LED light and that prepared with 3D DLS printer (*i.e.* fully crosslinked) were also characterized by spectroscopy (FTIR-ATR, Raman) and thermal analyses (DSC, TGA, DMA). The equipment used and the experimental procedure details are described in the SI file.

2.5.2. Characterization of thermoset copolymers upon 405 nm light irradiation and after complete curing

The curing kinetics of resin **c** was evaluated with rheology tests and Raman spectroscopy. In order to monitor the photopolymerization reaction and to determine a proper irradiation time per layer in the 3D printer, an indirect method was used, the shrinkage of pieces in a rheometer. Shrinkage was determined as the reduction of the gap sample from the beginning to the end of the experiment, following Eq. 2:

$$Shrinkage\ (\%) = \left(1 - \frac{gap_E}{gap_0}\right) \times 100 \qquad \text{(Eq. 2)}$$

In this way, a 50 µm layer of the liquid composition **c**, prepared using monomer **20**, was placed between the glass holder at the base and the aluminum plate. As the contact area of the plates with the sample is much higher than the air-sample area, oxygen inhibition will be negligible. The rheometer records the gap of the layer in real time as it shrinks in the curing process, triggered by the activation of the 405 nm LED, switched on 10 s after starting the experiment. This experiment helps to approximately determine the time that will be needed in order to print 50 µm layers by DLP. The results were plotted as a reduction of the gap layer (in µm) versus time (in seconds).

Raman measurements were performed *in situ* in separate experiments. They were carried out on a BWTEK dispersive i-Raman spectrometer equipped with a TE Cooled Linear Array detector and laser, using the 785nm light source (section 2.2.2, SI).

Stress-strain tensile measurements were also performed with dumbbell specimens printed with the 3D DLS printer, as mentioned before. Details of the experimental procedure are given in section 2.2.3 (SI file).

The sample crystallinity was evaluated by X-ray diffraction (XRD) and the morphology of the cured surface was evaluated with atomic force microscopy (AFM) (section 2.2.4, SI).

In a similar way as in the DLP process, for biodegradability and cytotoxicity studies, only one composition of the cured acrylate copolymer was chosen, corresponding to the material **C** (Table S1). Enzymatic degradation and cell viability studies are reported in sections 2.4 and 2.5, respectively, in the SI file. For biodegradation, the *Rhizopus oryzae* lipase enzyme was tested. For cellular viability, human osteoblast MG63 cells were employed and two approaches were considered: indirect and direct cell viability tests, due to the fast biodegradation of the prototype samples belonging to material **C**.

3. Results and discussion

3.1. Preparation of novel acrylamide monomers and acrylate copolymer thermosets

A solubility study was performed with all six new acrylamide resins to obtain a homogenous liquid mixture, which could eventually be used later in a photocuring 3D printer, aiming to obtain non-toxic and biodegradable materials. Despite the relatively low molecular weight of the monomers **18**-**23**, liquid low molecular weight polyethylene glycol diacrylate ($PEGDA_{250}$) was not sufficient to solubilize the monomers. Dimethyl acrylamide (DMAM) was added as a reactive solvent to ensure obtaining a homogeneous and transparent solution. Importantly, both poly-PEGDA[24] and poly-DMAM[25–28] have been used in biocompatible resins and they have reactive groups similar to the synthesized monomers, namely acrylates and acrylamides, being the former bifunctional and the later monofunctional. Moreover, a slightly high concentration of UV absorber was necessary to improve the printing resolution. This UV absorber proportion was based on the reactivity of the prepared resins, determined by photo-rheology (section 2.2.2, SI) and the target to print 50 μm thick layers with a 3D DLP printer.

Solid samples were obtained within seconds from all the six acrylamide monomers (**18**-**23**) synthesized, confirming fast photopolymerization of the acrylamide groups with $PEGDA_{250}$ and DMAM co-monomers, without any noticeable difference of reactivity among them (Figure 1). Therefore, the acrylate thermoset materials were successfully obtained in a solid state and proper crosslinking was checked after physical-chemistry characterization. The procedure could be translated to the 3D DLP printer because the same wavelength was applied (405 nm), which is a purple light at the limit of visible light with near UV irradiation.

As it will be further discussed in the next sections, the six monomers (**18**-**23**) provided pre-cured resins and cured materials with very similar properties. The main differences are in the physical state and solubility of the monomers, being the more flexible leucine-derivatives **21**-**23,** more waxy and easy to dissolve (see section 3.4), whilst phenylalanine-derived monomers **18**-**20** provided more rigid materials due to the presence of the aromatic rings. However, we could not find a clear influence in these properties which would be attributed to the spacer [(*E*)-butene diol, ethyleneglycol, diethyleneglycol]. The acrylate molecules length and the presence of C=C non-terminal groups, among other parameters, determine the crosslink density of the polymer and its stiffness.[29] Some discussion about those aspects are included in the dynamic thermal analysis (next section).

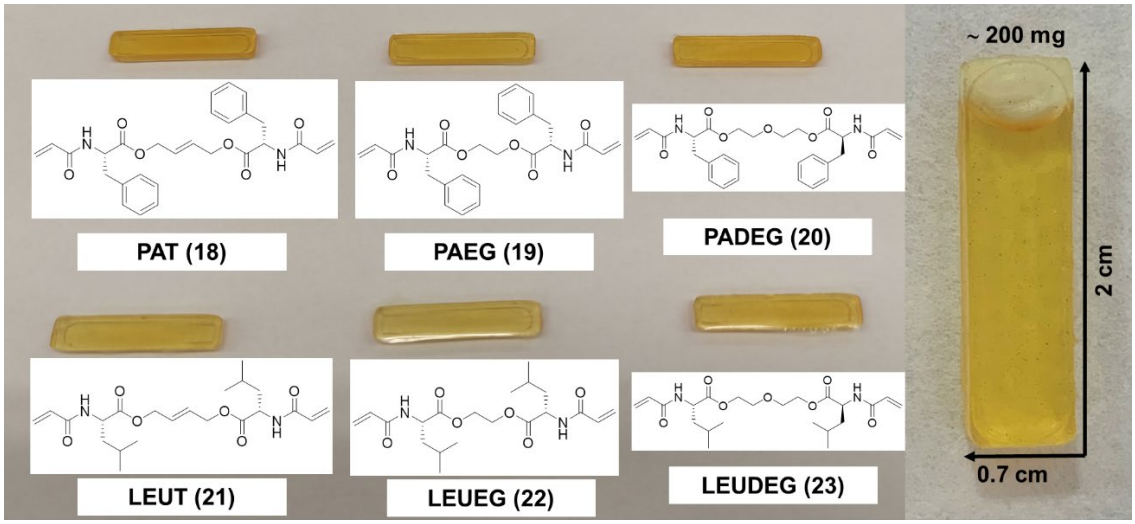

Figure 1. Photographs of solid samples obtained with the acrylamide monomers synthesized in the present study and cured under UV light of 405 nm (LED). On the right, a detail of one cured specimen has been shown.

3.2. Thermal and thermomechanical analyses of acrylamide-PEGDA-DMAM copolymers

The new monomer resins were designed to be cured with light irradiation, either in the more energetic visible range (*e.g.*, blue to violet, < 460 nm), or in the near UV region (*e.g.*, UVA region, 315-400 nm). However, they can also polymerize by applying heat, since the photoinitiator homolytically cleaves when it receives sufficient thermal energy to form the radical promoter. The building of new covalent bonds releases heat, thus, the exothermic energy produced by curing acrylates and acrylamides can be measured by

DSC analysis. The enthalpy (ΔH) evolved during the polymerization was calculated by integration of the calorimetric signal. The glass transition temperature (T_g) of the new acrylate thermosets was determined as the temperature of the halfway point of the change in the heat capacity of the material when it varies from a glassy to rubbery state of fully cured samples (Table 1).

In this work, two different functional groups react during the curing process, acrylates from PEGDA and acrylamides from the large monomers **18-23** (showed in Figure 1) and short DMAM molecules. It is reported that the usual heat enthalpy evolved by acrylate groups is about 70-80 kJ/mol,[30] while in the case of acrylamides, which are more energetic, this value rises up to 230 kJ/mol.[31] However, since our formulation contains different components and reactive groups, the results are presented in J/g and were found to be in the range of 400-600 J/g (Table 1).

DSC curves (Figure S4a, SI) show one exotherm peak for all the formulations. The more noticeable difference is the starting polymerization temperature of copolymer **c**, which is about 70°C, 20 ºC lower when compared to the other samples, also showing a fast-curing behaviour. The T_g's of all the samples, with all the curing and post-curing processes, showed similar values in the range of 120-125 °C, indicating that they are rigid at room temperature.

Acrylates and acrylamides in general, and more specifically in our case, which contain several ester, ether and amide groups from PEGDA, and, to some extent the synthesized monomers **18**-**23** and DMAM units, have an intrinsic affinity for water and they are therefore highly hygroscopic.[32,33] However, only a slight decrease of 1-2 wt. % of the initial mass was observed by TGA (below 50-150 °C) for all the cured samples tested (Figure S4b). Then, the onset temperature of the second degradation decay, which occurs in a single step, was taken as the degradation temperature of the acrylate samples. The thermal stability found is in the range of common acrylates, about 250 °C, reaching the maximum for samples **C** and **D**, with 277 °C and 283 °C respectively.[34] As it can be seen in Figure S4b, the maximum degradation rate is practically the same for all the samples at about 400 °C, denoting that the cured samples present a regular structure. Furthermore, the percentage of the final residue was also similar for all the samples, ranging from 7 to 9 %.

Table 1. Calorimetric and thermogravimetric data of the different copolymers prepared.

Liquid blend	ΔH[a] (J/g)	T_{max}[b] (°C)	T_g[c] (°C)	T_{SD}[d]/$T^*_{2\%}$[e] (°C)	Char yield[f] (%)
a	485	131	123±1	248±8 / 325±1	9±1
b	607	124	124±2	282±12 / 343±2	8±1
c	526	109	121±1	274±4 / 354±7	7±1
d	560	129	125±3	282±6 / 323±2	7±1
e	408	131	125±3	268±3 / 342±2	9±1
f	464	137	121±1	277±7 / 346±2	8±1

[a] Enthalpy evolved during the curing by a gram of mixture by DSC. [b] Temperature of exothermic peak, determined by DSC. Only one analysis was conducted. [c] Glass transition temperature of samples, determined by DSC, after complete curing of pieces, outside the device. The values are the average from 3 replicates; the ranges provided indicate a confidence level of 95%. [d] Temperature onset of the start of the degradation of the fully cured samples **A**-**F**, determined by TGA; the value is the average from 3 replicas; the ranges provided indicate a confidence level of 95%. [e] $T^*_{2\%}$ refers to the temperature at which 2% of the mass of the sample has been lost, considering as initial weight that of the sample once it has lost the initial weight between 50-150 °C, which is attributed to water loss; the value is the average from 3 replicas; the ranges provided indicate a confidence level of 95%. [f] Char residue at 600 °C under nitrogen atmosphere of the fully cured samples **A**-**F**, determined by TGA; the value is the average from 3 replicas; the ranges provided indicate a confidence level of 95%.

The dynamic mechanical analysis (DMA) of the different compositions **A-F**, lead us to confirm the effect of the addition of the new acrylamide monomers (compounds **18-23**) in Young's modulus and the loss to the storage energy (tan δ), compared to the respective homopolymers (poly-PEGDA and poly-DMAM) (Table 2). There is a considerable difference in the rigidity of the materials. Poly-DMAM, with only one C=C functional group in its structure, forms a linear thermoplastic polymer, which translates into a low rigidity modulus, in the span of 1 GPa. On the contrary, poly-PEGDA homopolymer, with two functional C=C groups, results in a crosslinked polymer network with Young's modulus that is nearly double than that of poly-DMAM homopolymer. When the new acrylamide monomers, synthesized in the present work, are introduced in the copolymer formulation, we observe a clear improvement in this property, reaching values of about 2.5 GPa for phenylalanine derivatives **A**, **B** and **C**, and about 2.3 GPa for leucine-derived materials **D**, **E**, and **F**. The difference is probably explained by the presence of aromatic rings in phenylalanine, which reduce the mobility of the chains.

Similar conclusions as in the previous case of the Young's modulus (*E*) can be derived from the *tan δ* values (T_g in Table 2). While the T_g of poly-DMAM homopolymer is 66 °C and for poly-PEGDA is 113 °C, in formulations that incorporate 18 wt. % of the different acrylamide monomers **18-23**, this value rises up to around 155 °C. Furthermore, besides the enhancement of the mechanical properties of the materials, the results point to a good integration of all the components within the matrix. This is proved by the width at half height (HH) of *tan δ* peak, presented in Table 2, since narrower values imply higher homogeneity of the network formed.[35] The values obtained are consistent with the temperature of thermal post-curing chosen to ensure the maximum degree of conversion, slightly higher than the T_g and far away from the starting thermal degradation temperatures obtained by TGA (Table 1).

From the values of the storage modulus at the rubbery state ($E'_{rubbery}$, Table S2), it is possible to calculate the molecular weight between crosslinks (Mc). There are a number of references in the literature reporting using the modulus measured within the rubbery plateau region to quantitatively calculate the polymer crosslinking densities.[36,37] As can be seen from the Figure S5, the measured rubbery plateau modulus increased with increasing the degree of crosslinking of the samples. In the meantime, the glass transition measured with DMA is also observed to shift to higher temperatures if compared to the homopolymers (Table 2). As it was expected, the longer diethyleneglycol linker in the monomers **20** and **23** provides higher Mc values (Table 2). Such high cross-linking densities translate in remarkably stiff and hard materials. The stiffness found in these materials is translated into the tensile strain that they can stand (see section 3.6, Figure 3). By other hand, the presence of the aromatic unit in phenyalanine acrylamide-derived compounds, compared to aliphatic ones, seems to have low influence in the crosslinking degree and thermal properties. For instance, Becker and co-workers have reported the DLP of biodegradable fumarate-based triblock copolyesters, with different proportions of ABA monomers and methylene lengths, crosslinked with a three-functional thiol monomer, obtaining a crosslinked star copolymer.[22] By DMA analysis they also found that higher storage modulus are achieved for copolymers with enhanced crosslinking degree (DC). The compositions with the highest amount of thiol units and lower concentration of poly(propylene fumarate) repeating units had the highest DC. The rate of hydrolytic degradation was also strongly dependent on the molecular weight of the backbone chains, the overall cross-link density, which in this case was controlled by varying the thiol amount.

Table 2. Thermomechanical data of the different compositions **A-F** and compared with pure homopolymers. All data were derived from DMA analysis.

Cured material	E[a] (GPa)	T_g[b] (°C)	Width at HH[c] (°C)	Mc (g·mol^{-1})[d]
Poly-DMAM	0.95 ± 0.12	66	-	-
Poly-PEGDA	1.73 ± 0.09	113	29	67
A	2.55 ± 0.11	151	22	280
B	2.62 ± 0.12	154	21	288
C	2.54 ± 0.13	150	22	305
D	2.35 ± 0.09	155	27	271
E	2.41 ± 0.10	158	24	275
F	2.17 ± 0.15	152	24	290

[a] Young's modulus tested at 30 °C in a DMA with a controlled force experiment. The values are the average from 3 replicas and the ranges provided indicate a confidence level of 95%. [b] Temperature of tan δ peak determined at 1 Hz in an oscillatory experiment by DMA. [c] Width at half height of tan δ peak. [d] Molecular weight between crosslinks (Mc) was deduced from the equation S3 (section 3.1, SI file). Due to the time required to perform these experiments, only one analysis was conducted with each sample.

3.3. Chemical conversion of acrylate/acrylamide monomers characterized by FTIR and Raman spectroscopies

The liquid blends **a-f** and the completely cured materials **A-F** were evaluated by attenuated infrared analysis (FTIR-ATR) to determine the degree of chemical conversion. Figure 2a presents a comparison of the FTIR spectra of the resin before (copolymer **c**) and after the curing process (cured material **C**) as one representative example.

Usually, acrylates present a peak in the range of 1610-1620 cm^{-1}, which corresponds to the carbon-carbon double bond stretching (C=C) of the α,β-unsaturated carbonyl moiety. Close to this peak, the carbonyl stretching of the acrylamides (C=O) at *ca.* 1660 cm^{-1}, and at about 1710-1740 cm^{-1} the peak corresponding to the carbonyl stretching (C=O) of the acrylate esters can be observed (Figure 2a). After curing, the peak of the now saturated ester does not change substantially, appearing at 1720-1740 cm^{-1}; moreover, the peak corresponding to the saturated amides at 1620-1650 cm^{-1}overlaps and masks the possible presence of unreacted alkene, making it impossible to evaluate the polymerization conversion in this zone. Nevertheless, a double peak in the range of 826-780 cm^{-1}, which is present in the resin and not observed in the cured material, was

followed (inset of Figure 2a), which is likely due to an out-of-plane vibration of the C-H of the double bond (=CH).

Table 3 shows the calculated conversions of the different copolymers cured in the 3D printer. For leucine-derived materials (**D**-**F**, using monomers **21**-**23**) formulations, no reference peak could be found to correct the conversion, but all the polymerizations reached a high degree of conversion after the thermal post-curing treatments, with about 99 % of reactant groups consumed. It is interesting to note that the conversion, when the resin was cured in the 3D printer, is slightly increased, probably due to the thin thickness of each layer (50 μm) controlled by the layer-by-layer curing process, which helped to reach almost 100 % of the curing.

Table 3. Degree of polymerization conversion determined by FTIR-ATR spectroscopy.

Cured material	Conversion (%)	Conv. with correction (%)
A	98.7	98.9
B	99.3	99.2
C	98.8	98.9
D	99.6	-
E	99.0	-
F	99.5	-
C (3D-printed)	99.8	99.6

The curing kinetics were evaluated with rheology test and Raman spectroscopy of the uncured liquid resin **c** and a completely cured sample **C.** The Raman spectra are represented in Figure 2b. A good resolution signals were obtained using 100% of 405 nm LED-lamp intensity for 30 s. Despite the most characteristic peak to follow the conversion of acrylates is the acrylic double bond (C=C) in the range of approximately 1600 cm^{-1}, in our case, similarly to what was observed in IR spectroscopy, it was not possible to follow the reaction at this wavelength due to overlapping of peaks of C=O from amide and ester groups, as shown in Figure 2b. For this reason, an absorption band at 761 cm^{-1}, present in the uncured resin and absent in the cured material, was selected to evaluate the polymerization reaction. This band corresponds to the bending angle of =C-H bond of the acrylate groups.

To determine the acrylate-acrylamide consumption, both peak area and peak height can be taken into account.[38][39] Therefore, the reduction in the area and height of the absorption band at 761 cm^{-1} (inset of Figure 2b) was measured. It was found a conversion of 95 % of polymerization after approximately 90 s of light irradiation (~150 s from the beginning of the experiment). The evolution of the peak height and peak area decrease with time can be seen in Figure S6, from SI, and both presented the same behavior.

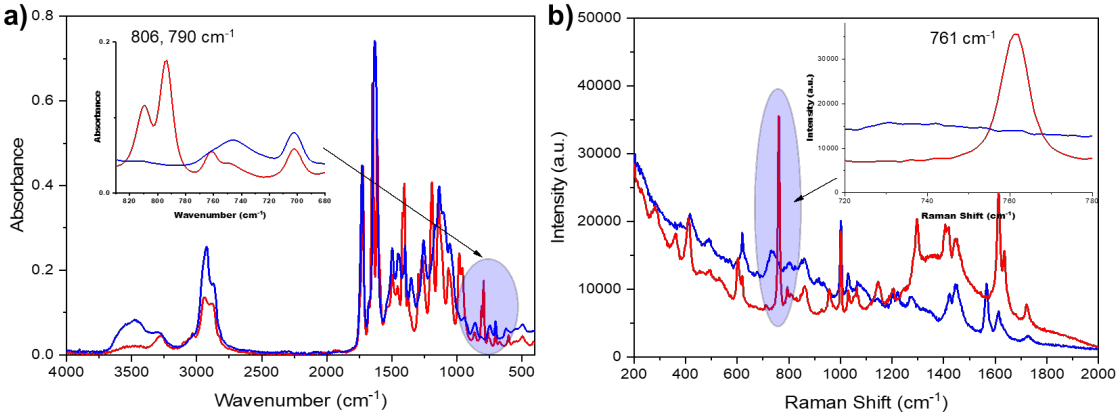

Figure 2. (a) Comparison of FTIR-ATR spectra of liquid composition **c**, containing monomer **20** (red curve), before curing, and the cured material **C** (blue curve). Inset image corresponds to the wavenumber range of 826-780 cm^{-1} showing the reduction of 806 cm^{-1} and 790 cm^{-1} peaks after sample curing. (b) Raman spectra of liquid composition **c**, containing monomer **20** (red curve), before curing, and cured material **C** (blue curve). Inset image represents the reduction of absorption peak at 761 cm^{-1}.

Altogether, this information led us to conclude that the new acrylamide compounds can be useful co-monomers for DLP printers when combined with appropriate co-monomers and little amount of BAPO as a photoinitiator.

3.4. Selection of the most prominent acrylamide monomer for 3D printing

In order to test the liquid formulations in a commercial 3D DLP printer, higher amounts of material would be needed (*ca*. 150 mL of liquid resin, which corresponds to *ca*. 30 g of monomer). Furthermore, some other tests would be desirable before committing to printing in the 3D printer (*e.g.* rheology tests, and study of the printing parameters, among others). For this reason, we analyzed which of the synthesized monomers would be the most appropriate to scale up.

As commented in section 3.1, there are some structural-derived features that guided our choice of the preferred monomer. When using L-Leucine as the amino acid, we noticed that the final monomers (compounds **21**, **22**, and **23**) were waxy materials or viscous syrups, with a low tendency to crystallize. Despite the fact that these monomers readily and easily dissolve in the mixture of PEGDA and DMAM co-monomers, they present some drawbacks: i) their thermomechanical behavior does not provide advantages compared to the phenylalanine counterparts **18**, **19**, and **20**; ii) they would be more difficult to purify in a subsequent scale-up, and their manipulation, weighting and solvent removal would be more cumbersome. Thus, the monomers **21**-**23** derived from leucine, which provided highly viscous materials, were discarded.

On the other hand, the monomer products derived from L-phenylalanine (**18**, **19** and **20**) appeared as white solids, which would simplify their isolation and purification. However, they also have the drawback of slower solubilization than leucine derivatives. To enhance solubility, the formulations were stirred at 60 °C. The resulting homogeneous solutions were stable when cooled to room temperature.

Once the thermomechanical characterization (DMA) was completed, we proceeded to select the best candidate to scale-up the monomer synthesis. In this sense, most thermomechanical properties are similar, although blend **c**, which incorporates the acrylamide **20** as a monomer, seems to react faster since the DSC results indicate a lower initial polymerization temperature compared with the other blends (see Table 1). In addition, monomer **20**, incorporates diethylene glycol as diol, which resembles more the PEGDA used in the formulation, and, in terms of economic aspects, it is an affordable diol. Thus, for the proper use of the 3D printer, different tests were carried out in order to obtain high-quality printed materials with formulation **c**, and the other blends have not been further progressed.

3.5. Rheology tests

In order to monitor the kinetics of the photopolymerization reaction and to determine a proper irradiation time per layer in the 3D printer, the shrinkage method was used (Eq. 2). Shrinkage is one of the most important drawbacks of curable polymers, since it affects the final shape of the components (dimensional stability) and produces internal stresses, which can generate defects such as fractures in large dimensional samples. The shrinkage percentages of a liquid resin converted into a solid, during the polymerization process, can be related to the degree of polymer conversion.[40–42]

Figure S7a shows the gap variation during sample irradiation (405 nm LED activated at 10 s) for the resin **c**, prepared with monomer **20**. The experiment, performed at room temperature, showed a high rate of radical polymerization. From the plot, it is deduced that there is an inhibition time of approximately 4 s from the beginning of the irradiation, after which time the polymerization process kicks off quickly. Thus, after 24 s of irradiation, the gap achieved its minimum, and although the experiment was prolonged for 300 s, the resulting gap value was constant, which indicates that a high degree of conversion has been achieved and giving a total shrinkage of 12.6%. Moreover, this graphic indicates that the irradiation per layer should be in the range of 20 s. The values found for the shrinkage are in the usual range for common acrylates.[43] For comparison, the experiment was repeated using a gap of 400 µm, obtaining practically analogous time to start the reaction and proving that the shrinkage is not dependent on the sample gap used (Figure S7b).

The relatively high amounts of PEGDA and DMAM in the formulation can account for a significant part of the shrinkage observed since pure PEGDA shrinks up to ~14%,[44] whilst DMAM does so up to 16.9%.[45] Several methods to reduce the shrinkage of resins have been reported, but they generally reduce reactivity and/or light penetration.[42] Although this is not the aim of the present study, we do not discard improving such properties of the best acrylate/acrylamide composition in the future.

The polymerization kinetics evaluated by in situ by Raman spectroscopy were already discussed in section 3.3.

3.6. DLP printing and test specimens' characterization

As the intensity of the printer is fixed, the printing parameters, *i.e.* layer thickness and exposure time per layer, were optimized by performing a Jacobs working curve (see section 3.4 from SI for details).[46–48] The results derived from equation S3 suggest an exposure time of about 8-9 s for a 50 µm layer. However, in our case, when constructing the working curve, we observed that a minimum of 15 s was needed in order to have a measurable film (Figure S8). These values, combined with the learnings from the photo-rheometer experiments, indicated that an irradiation time of 20 s per layer should be selected in the 3D printing of the acrylate/acrylamide copolymer.

Once the printing parameters were determined, tensile test samples were printed in three different directions (section 2.2.3, SI, Figure S3), due to the possibility of obtaining

anisotropic behaviour of printed materials, which can be as high as 30% in some cases.[49] At least six samples were tested for each material. The maximum stress (σ_{max}) and the deformation at break (ε_b) were determined from the failure point, as can be seen in Figure 3a. The elastic modulus *E* was calculated from the slope of the curve in the initial linear part of the curve (taken between 10 and 20 N of the device force) (Table 4).

As it can be deduced from Table 4, the printing orientation for this material is practically negligible, despite the fact that usually the intra-laminar bonds formed during the curing are stronger than the inter-laminar bonds, since the superior layers are built onto the previous one as an adhesive joint. The study found that the material **C**, which incorporates monomer **20** within its formulation, showed a notable isotropy in terms of rigidity and deformation at the break. The Young modulus values are in the range of 2 GPa, which is similar to that found with DMA analysis (Table 2).

These results evidence an excellent copolymer mechanical behavior and good selected parameters at the printer machine, including exposure time per layer, layer thickness and UV absorber concentration. Only the strain at break and ultimate tensile stress needed by the device for a constant deformation present slight differences, always inside the tolerance of results deviation. The tiny diminution of the strain and the enhancement of maximum stress required can mean an imperceptible augmentation of thermoset brittleness for samples printed in Z direction.

After rupture, the morphology of the fractured zones was inspected with SEM. Figure 3b shows an example of a typical fragile rupture, inherent to brittle thermoset polymers. From a completely flat surface where the dramatic failure occurred, departed straight lines of rupture, with small signs of plastic deformation (Figure 3b). It can be observed that no different phases are present within the material, as also observed in AFM images (see section 3.7 below), which confirms the excellent integration of all the components of the formulation, as previously observed by thermomechanical analysis. The precision of the 3D-printed thickness among the different layers can be appreciated in Figure 3c. The space between layers matches perfectly with the dimensions demanded by the printer, which again, confirmed the good curing parameters selected for this formulation.

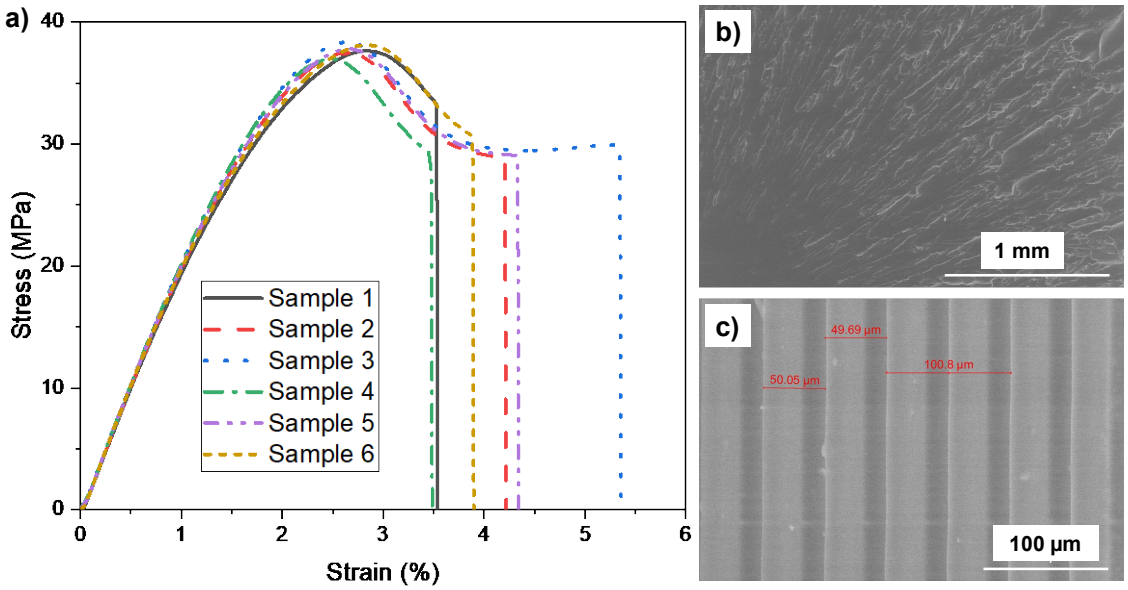

Figure 3. a) Stress-strain curves of material **C** printed in plane; b) micrograph of in plane printed sample of **C**. b) SEM micrograph of cross-section fragile rupture for material **C** printed in plane (low magnification, 80×); and c) lateral view of material **C** showing the different layer thickness of 50 µm (high magnification, 600×).

It is interesting to notice the role of the synthesized monomer **20** in the mechanical properties of the dumbell-shaped samples. A sample without the monomer was 3D-printed to compare its behaviour (Table 4). A reduction of 31% of the rigidity is observed in the absence of monomer **20**, and the deformation at break increases from 4.1 to 5.1%, slightly reducing the brittleness of the material at the expense of mechanical strength. Therefore, despite the relatively low concentration of **20** in the formulation, its addition translates into a significant improvement in the mechanical properties of the material.

Table 4. Data extracted from tensile test experiments for 3D-printed dumbell-shaped samples, using monomer **20** in the formulation.

Cured material	E[a] (GPa)	Strain at break[b] (%)	Tensile strength[b] (MPa)
C in plane	2.10 ± 0.34	4.1 ± 0.5	37.7 ± 0.4
C in X	2.08 ± 0.42	4.1 ± 0.4	37.8 ± 0.8
C in Z	2.09 ± 0.61	3.7 ± 0.7	39.3 ± 1.9
PEGDA/DMAM (blank; in plane)	1.44 ± 0.68	5.1 ± 0.4	22.7 ± 1.2

[a] Young's modulus determined in the initial linear curve of the strain-stress graph (10-20 N). [b] Deformation when samples break and the maximum tension required by the device to constantly deform the sample, obtained from the tests. The values are the average from 6 replicas and the ranges provided indicate a confidence level of 95%

As can be seen, in Figure 4, we were able to print the test specimen with very high resolution and also a model of the monumental Basílica i Temple Expiatori de la Sagrada Família in Barcelona (designed by Antoni Gaudí architect).

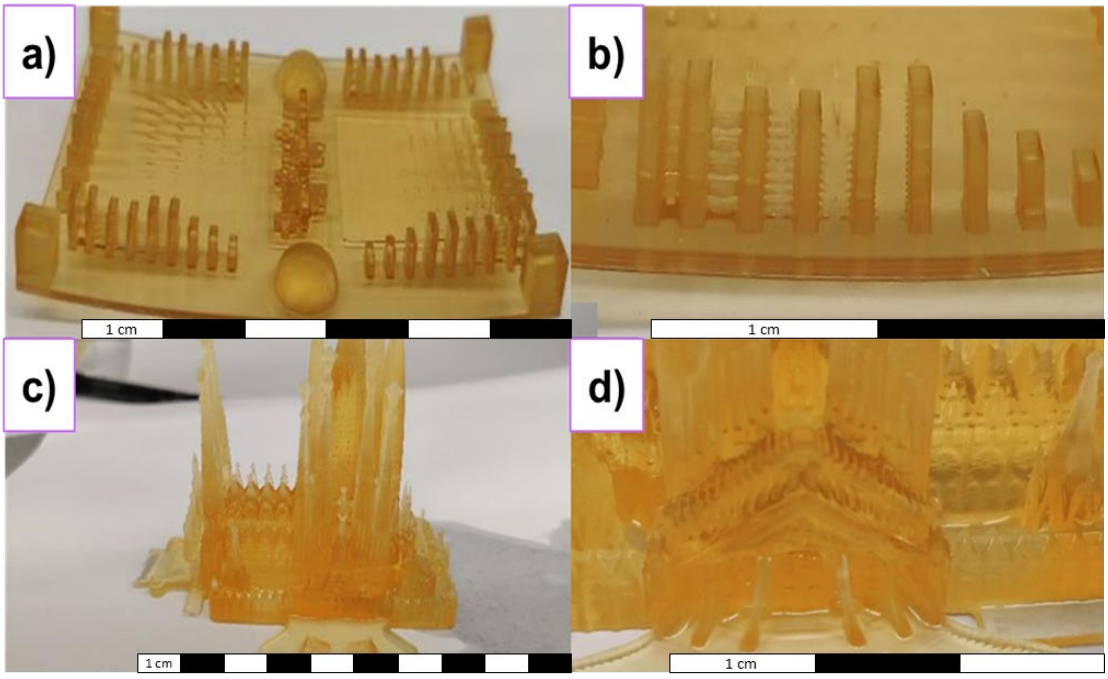

Figure 4. Examples of some prototypes printed with DLP 3D printer employing the resin formulation **c**, which includes the acrylamide **20**, PEGDA and DMAM co-monomers: a) resolution piece. b) Detail of the dimensional stability of columns of the resolution piece; c) complex model of Gaudi's Sagrada Família; and d) detail of one of the facades of the monument (Glory façade).

3.7. Biodegradation and cytotoxicity of biodegradation products of compound C

The rise of 3D manufacturing and the continuous generation of plastic waste from such processes undoubtedly highlights the need to explore methods for recycling and controlled decomposition of said waste. A high number of studies has been raised regarding the recyclability of 3D-printed pieces combining biodegradable and non-biodegradable polymers,[50,51] and even with combinations of biodegradable polymers with enzymes to accelerate the degradability of the pieces.[52] However, few works address the evaluation of the toxicity of biodegraded products.[40,53,54] Oskui *et al*.[53] have demonstrated that synthetic acrylate polymers, printed by using stereolithography and post-treated with UV irradiation, have reduced toxicity when in contact with aquatic organisms (zebrafish) if compared to the samples without post-printing treatment. Thus, the key to such a result was to have a well-cured and washed acrylate sample. In this study, we performed *in vitro* tests to approach the biodegradability and the cytotoxicity of the DLP 3D-printed and post-cured pieces of thermoset **C**.

The selection of the functional groups presents in the monomers (amide, ester, and particularly the vicinal alkoxy ether moieties of diethylene glycol and polyethylene glycol) used to obtain the thermoset, make the resulting cured material **C** to have a high affinity to water (see Table S3 with water uptake data). The biodegradability was assessed in phosphate buffer saline solution (PBS), without and with *Rhizopus oryzae* lipase enzyme. Figure 5 depicts the aspect of the samples before and after immersion in PBS/lipase solution at 37ºC and 90 rpm, according to the immersion time. In 7-14 days, the samples started to break into small pieces until they reached the aspect of a powder in 90 days. The evolution of the degradation of the pieces in the PBS solution is depicted in Figure S9.

The degradation process seems to start and to follow a hydrolytic mechanism, rather than enzymatic, since the samples without enzyme presented the same tendency of weight loss as those with the enzyme (28.5 ± 3.5 % and 26.6 ± 5.0 %, without and with lipase medium, respectively, after 90 days). This is probably due to the mentioned high water uptake and the fact that the sample disaggregates into tiny fragments with time, *i.e.* large contact area also translates into faster biodegradation of the small pieces. The late statement is the reason why, in composting assays, the plastic must be crushed before testing.[50]

Lipase from *Rhizopus oryzae* is frequently employed for *in vitro* enzymatic degradation of polyesters. However, the results obtained for phenylalanine-derived thermoset cannot be compared with the very fast degradation of polyesters homopolymers.[32,55]

Nevertheless, taking into account that this is a synthetic acrylate polymer produced by the DLP process, and having demonstrated that the printed layers are well cohesive (reproducible stress-strain curves and SEM cross-section images), the degradation rate is very positive. The powdered substance can be filtered and can be upcycled into new products, if desirable.

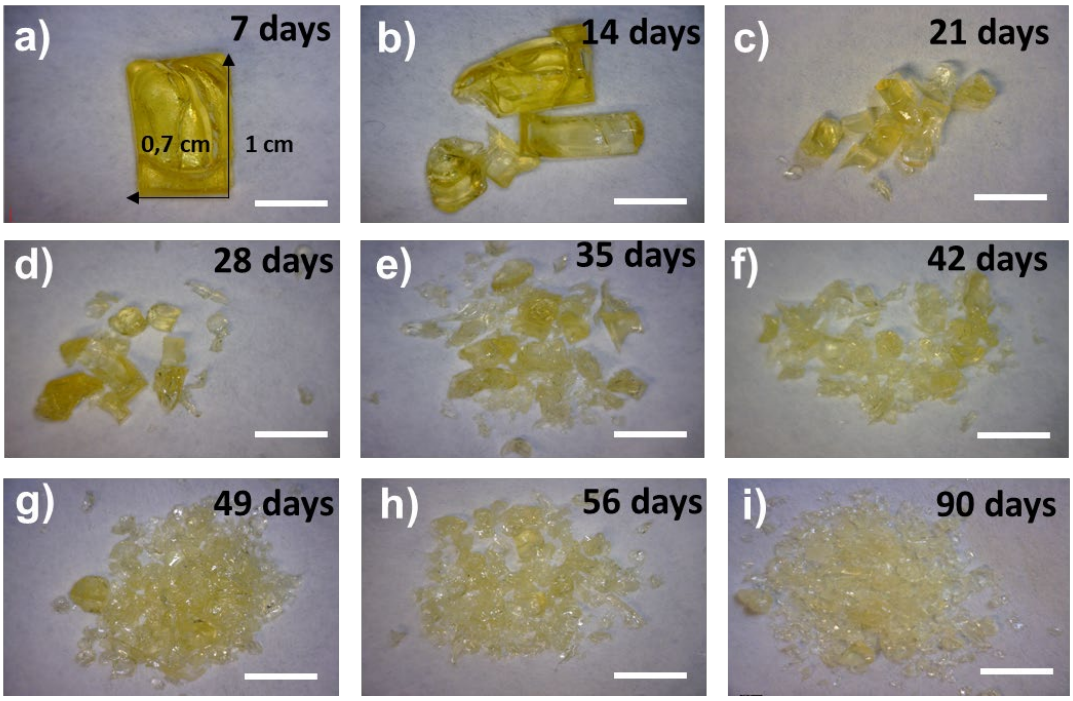

Figure 5. Photographs of biodegradation products from PADEG-PEGDA-DMAM (material **C**), after incubation of 3D-printed rectangular pieces in PBS/*Rhizopus oryzae* lipase medium. Scale bars refer to 0.5 cm.

As the absorption of water and degradation of compound **C** are high, the morphology and crystallinity of one sample were evaluated to check if this behaviour originates from different amorphous and crystalline phases. AFM images revealed homogenous surface as indicated by Figure S10. Several zones of the 3D-printed samples were evaluated. Moreover, there is no evidence of crystalline phases in XRD plots. Instead, the material presented two amorphous phases (Figure S11).

Therefore, the fast degradation rate can only be attributed to the nature of the thermoset polymer.

We then turned our attention to certify if the biodegraded products of our thermoset material are not toxic, which is of outmost importance for printed parts disposal. One strategy to do so is the indirect evaluation of cells that are alive after 24h and during 7 days. Thus, degradation products of material **C** were screened for cytotoxicity using MG63 osteoblast cells. Cell viability was evaluated in the presence of 24h- and 7days-extracts (dilution series), as exposed in Figure 6. The rapid degradation of the samples, also observed in cell culture media at 37 °C, only after a few days of incubation, precluded further characterization. However, the results obtained for the indirect cell viability test verified the cytocompatibility of material **C** (Figure 6). Indeed, MG63 relative cell viability was high for the whole concentration range when exposed to 24h-extracts as no dose-dependent cytotoxicity was observed (Figure 6a). In fact, even though more concentrated dilutions showed lower values, cell viability was above 82% in all cases, which evidences the cytocompatibility of compound **C**. Regarding 7d-extracts, a similar response was observed with relative cell viability values higher than 92% (Figure 6b).

We should mention that cell proliferation does not occur on the surface of material **C**, probably due to the extremely smooth surface of the sample (see Figure S9) proved by AFM. On the other hand, indirect measurement of cell viability by evaluation of the products delivered to the medium indicated that the samples were not toxic to this cell line, as explained above. This fact led us to conclude that the biodegraded products from thermoset **C** can be "friendly" with other microorganisms if in contact with them. However, additional standard tests will be necessary to validate the product as a good material for upcycling as composting, for example. This step is being envisaged for future research work.

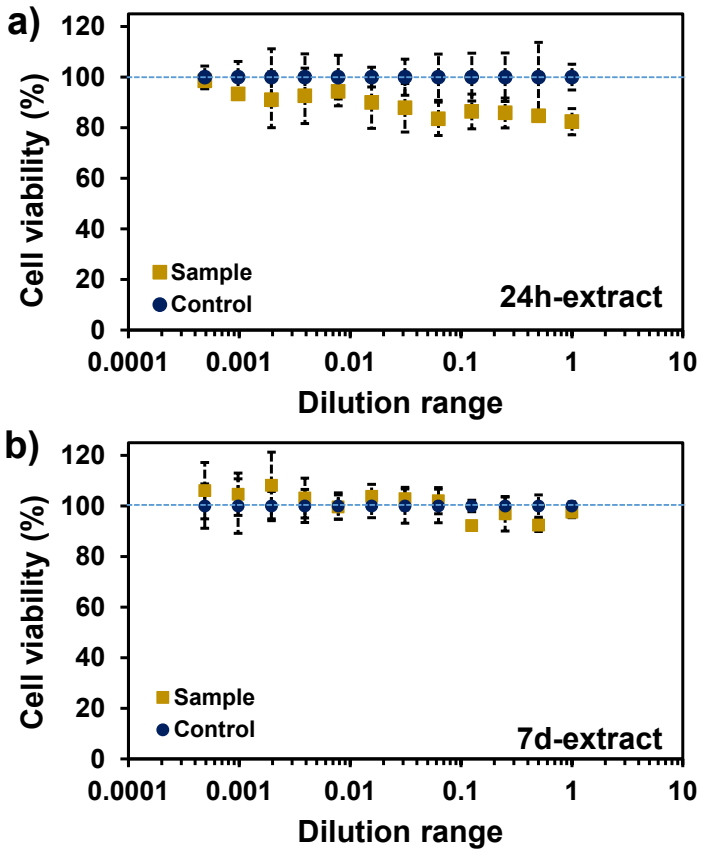

Figure 6. Relative cell viability for MG63 osteoblast cells after 48 hours when exposed to a dilutions series of a) 24h-extracts and b) 7days-extracts of compound **C**. In each case, 100% viability was established by DMEM-only extract as control.

4. Conclusions

The development of acrylate resins with fast curing time and good biodegradability properties is of utmost relevance to obtain prototypes with superior recyclability. In the present work, we have proven that α-amino acids are promising compounds to potentiate the biodegradability of acrylate plastics by introducing the acrylamide-ester functionalities to the polymer chain.

Stable formulations were prepared by combining the new amino acid-derived acrylamide monomers with two co-monomers commonly used in DLP or SLA printers, PEGDA and DMAM. Dog-bone specimens, as well as complex structure shapes, were generated with a DLP printer, by using 405 nm light, photoinitiator and photo-absorber molecules. The irradiation times were similar to commercial acrylate resins; however, two post-curing processes (further visible light irradiation at 460 nm and thermal curing)

were required to get completely cured samples, free of residual monomers that could cause problems of toxicity.

The mechanical properties of compound **C**, prepared from L-phenylalanine and diethyleneglycol, PEGDA, and DMAM, were superior to the same material without the amino acid-derived acrylamide. The L-phenylalanine monomer was able to improve both the rigidity and the storage modulus of the printed samples. In addition, the cured sample C was found to be isotropic, with mechanical properties not dependent of printing orientation. Moreover, compound **C** proved to have high hydrolytic degradation rate due to its affinity to water, being the degraded products leached to cell culture medium non-cytotoxic. Altogether, the results obtained open new frontiers for the development of more polyesters SLA products derived from amino acids.

Data availability

A supporting information file is supplied, which contains the main experimental procedures to prepare the new acrylamide-ester di-functional monomers, as well as the thermoset material characterization. Any additional information not included in the support file may be requested from the authors after a reasonable justification.

Acknowledgments

This work has been supported by the project (BASE3D 001-P-001646), which is funded by the European Regional Development Fund (ERDF), and has a total cost of 3.774.442,42€ of which 1.887.221,21€ (50%) are subsidized. M.M.P.-M. thanks the Ministerio de Educación y Formación Profesional for the Junior Beatriz Galindo Award (BG20/00216). The research leading to these results has received funding from ”la Caixa” Foundation under the grant agreement LCF/PR/PR20/51150010. We thank Prof. Silvia de la Flor from Universitat Rovira i Virgili for facilitating access to DMA, and Dr. Giandomenico Magagnano for initial studies with the UPEA polymer that led to the development of the new monomers. The Characterization Technologies Department (NMR, TGA, DSC, Rheometry, Raman, HRMS, Photophysics) and the Reaction Technologies Department of ICIQ (Mechanical Workshop) are kindly acknowledged.

Conflict of interest

Authors declare they do not have any conflict of interest.

References

[1] D. Rejeski, F. Zhao, Y. Huang, *Addit. Manuf.* **2018**, *19*, 21.

[2] M. Hong, E. Y. X. Chen, *Green Chem.* **2017**, *19*, 3692.

[3] N. Aurisano, R. Weber, P. Fantke, *Curr. Opin. Green Sustain. Chem.* **2021**, *31*, 100513.

[4] Y. Shi, J. Faludi, *Addit. Manuf.* **2020**, *35*, 101307.

[5] T. M. Lammens, M. C. R. Franssen, E. L. Scott, J. P. M. Sanders, *Biomass and Bioenergy* **2012**, *44*, 168.

[6] K. Guo, C. C. Chu, E. Chkhaidze, R. Katsarava, *J. Polym. Sci. Part A Polym. Chem.* **2005**, *43*, 1463.

[7] G. Ruano, A. Díaz, J. Tononi, J. Torras, J. Puiggalí, C. Alemán, *Polym. Test.* **2020**, *82*, 106300.

[8] G. Ruano, J. Tononi, D. Curcó, J. Puiggalí, J. Torras, C. Alemán, *Soft Matter* **2020**, *16*, 8033.

[9] S. I. Macías, G. Ruano, N. Borràs, C. Alemán, E. Armelin, *J. Polym. Sci.* **2022**, *60*, 688.

[10] V. S. D. Voet, J. Guit, K. Loos, *Macromol. Rapid Commun.* **2021**, *42*, 2000475.

[11] T. Matsuda, M. Mizutani, *J. Biomed. Mater. Res.* **2002**, *62*, 395.

[12] N. B. Palaganas, J. D. Mangadlao, A. C. C. De Leon, J. O. Palaganas, K. D. Pangilinan, Y. J. Lee, R. C. Advincula, *ACS Appl. Mater. Interfaces* **2017**, *9*, 34314.

[13] A. Cosola, R. Conti, H. Grützmacher, M. Sangermano, I. Roppolo, C. F. Pirri, A. Chiappone, *Macromol. Mater. Eng.* **2020**, *305*, 2000350.

[14] C. Warr, J. C. Valdoz, B. P. Bickham, C. J. Knight, N. A. Franks, N. Chartrand, P. M. Van Ry, K. A. Christensen, G. P. Nordin, A. D. Cook, *ACS Appl. Bio Mater.* **2020**, *3*, 2239.

[15] B. Zhang, S. Li, H. Hingorani, A. Serjouei, L. Larush, A. A. Pawar, W. H. Goh, A. H. Sakhaei, M. Hashimoto, K. Kowsari, et al., *J. Mater. Chem. B* **2018**, *6*, 3246.

[16] Q. Ge, Z. Chen, J. Cheng, B. Zhang, Y.-F. Zhang, H. Li, X. He, C. Yuan, J. Liu, S. Magdassi, et al., *Sci. Adv.* **2021**, *7*, 1.

[17] T. Xiao, Y. Chen, Q. Li, Y. Gao, L. Pan, F. Xuan, *Adv. Mater. Technol.* **2022**, *2201376*, 2201376.

[18] G. Gonzalez, A. Chiappone, K. Dietliker, C. F. Pirri, I. Roppolo, *Adv. Mater.*

Technol. **2020**, *5*, 2000374.

[19] A. Jandyal, I. Chaturvedi, I. Wazir, A. Raina, M. I. Ul Haq, *Sustain. Oper. Comput.* **2022**, *3*, 33.

[20] N. F. Zaaba, M. Jaafar, *Polym. Eng. Sci.* **2020**, *60*, 2061.

[21] M. Zhang, G. M. Biesold, W. Choi, J. Yu, Y. Deng, C. Silvestre, Z. Lin, *Mater. Today* **2022**, *53*, 134.

[22] A. Kirillova, T. R. Yeazel, K. Gall, M. L. Becker, *ACS Appl. Mater. Interfaces* **2022**, *14*, 38436.

[23] J. Huang, Z. Chen, C. Wen, T. Ling, Z. Chen, *Addit. Manuf.* **2022**, *59*, 103088.

[24] J. R. Choi, K. W. Yong, J. Y. Choi, A. C. Cowie, *Biotechniques* **2019**, *66*, 40.

[25] M. P. Algi, O. Okay, *Eur. Polym. J.* **2014**, *59*, 113.

[26] B. A. Zasónska, N. Boiko, D. Horák, O. Klyuchivska, H. Macková, M. J. Beneš, M. Babič, M. Trchová, J. Hromádková, R. Stoika, *J. Biomed. Nanotechnol.* **2013**, *9*, 479.

[27] J.-C. Yeh, Y.-T. Hsu, C.-M. Su, M.-C. Wang, T.-H. Lee, S.-L. Lou, *J. Biomater. Appl.* **2014**, *29*, 442.

[28] D. Ceylan Tuncaboylu, T. S. Yıldırım, *Polym. Bull.* **2019**, *76*, 5333.

[29] I. M. Barszczewska-Rybarek, *Materials (Basel).* **2019**, *12*, 4057.

[30] K. G. McCurdy, K. J. Laidler, *Can. J. Chem.* **1964**, *42*, 818.

[31] M. KT, S. P, *Org. Chem. Curr. Res.* **2016**, *4*, 2.

[32] M. T. Zumstein, D. Rechsteiner, N. Roduner, V. Perz, D. Ribitsch, G. M. Guebitz, H. P. E. Kohler, K. McNeill, M. Sander, *Environ. Sci. Technol.* **2017**, *51*, 7476.

[33] M. Cadenaro, T. Maravic, A. Comba, A. Mazzoni, L. Fanfoni, T. Hilton, J. Ferracane, L. Breschi, *Dent. Mater.* **2019**, *35*, e1.

[34] I. Isarn, L. Bonnaud, L. Massagués, À. Serra, F. Ferrando, *Polym. Int.* **2020**, *69*, 280.

[35] A. R. Kannurpatti, J. W. Anseth, C. N. Bowman, *Polymer (Guildf).* **1998**, *39*, 2507.

[36] I. M. Barszczewska-Rybarek, A. Korytkowska-Wałach, M. Kurcok, G. Chladek, J. Kasperski, *Acta Bioeng. Biomech.* **2017**, *19*, 47.

[37] K. P. Menard, N. R. Menard, *Dynamic Mechanical Analysis*, Boca Raton CRC Press, Boca Raton, **2020**.

[38] S. Parnell, K. Min, M. Cakmak, *Polymer (Guildf).* **2003**, *44*, 5137.

[39] R. Hardis, J. L. P. Jessop, F. E. Peters, M. R. Kessler, *Compos. Part A Appl. Sci. Manuf.* **2013**, *49*, 100.

[40] S. Salehi, F. Gwinner, J. C. Mitchell, C. Pfeifer, J. L. Ferracane, *Dent. Mater.* **2015**, *31*, 195.

[41] C. Schmidt, T. Scherzer, *J. Polym. Sci. Part B Polym. Phys.* **2015**, *53*, 729.

[42] L. F. J. Schneider, L. M. Cavalcante, N. Silikas, *J. Dent. Biomech.* **2010**, *1*, 1.

[43] J. Świderska, Z. Czech, A. Kowalczyk, *Polish J. Chem. Technol.* **2013**, *15*, 81.

[44] A. Al Mousawi, F. Dumur, P. Garra, J. Toufaily, T. Hamieh, F. Goubard, T.-T. Bui, B. Graff, D. Gigmes, J. Pierre Fouassier, et al., *J. Polym. Sci. Part A Polym. Chem.* **2017**, *55*, 1189.

[45] A. M. North, A. M. Scallan, *Polymer (Guildf).* **1964**, *5*, 447.

[46] P. F. Jacobs, in *Proc. Solid Free Form Fabr. Symp.* (Ed: H. L. Marcus), 3D Systems, **1992**, pp. 196–211.

[47] Y. Li, Q. Mao, J. Yin, Y. Wang, J. Fu, Y. Huang, *Addit. Manuf.* **2021**, *37*, 101716.

[48] M. Štaffová, F. Ondreáš, J. Svatík, M. Zbončák, J. Jančář, P. Lepcio, *Polym. Test.* **2022**, *108*, 107499.

[49] P. Biswas, S. Guessasma, J. Li, *Acta Mech.* **2020**, *231*, 503.

[50] S. Choe, Y. Kim, G. Park, D. H. Lee, J. Park, A. T. Mossisa, S. Lee, J. Myung, *ACS Appl. Polym. Mater.* **2022**, *4*, 5077.

[51] E. M. Maines, M. K. Porwal, C. J. Ellison, T. M. Reineke, *Green Chem.* **2021**, *23*, 6863.

[52] A. F. Greene, A. Vaidya, C. Collet, K. R. Wade, M. Patel, M. Gaugler, M. West, M. Petcu, K. Parker, *Biomacromolecules* **2021**, *22*, 1999.

[53] S. M. Oskui, G. Diamante, C. Liao, W. Shi, J. Gan, D. Schlenk, W. H. Grover, *Environ. Sci. Technol. Lett.* **2016**, *3*, 1.

[54] M. Moldovan, R. Balazsi, A. Soanca, A. Roman, C. Sarosi, D. Prodan, M. Vlassa, I. Cojocaru, V. Saceleanu, I. Cristescu, *Materials (Basel).* **2019**, *12*, 2109.

[55] K. Shi, J. Jing, L. Song, T. Su, Z. Wang, *Int. J. Biol. Macromol.* **2020**, *144*, 183.

Table of Contents

3D-printing of amino acid-derived and poly(ethylenglycol) diacrylate co-monomers with high degradability and mechanical integrity.